Diurnal, Seasonal, and Geomagnetic Activity Variations in the Occurrence of Decametre-Scale Irregularities in the Auroral and Subauroral Ionosphere

Murray L. PARKINSON, John C. DEVLIN, Peter L. DYSON, Mike PINNOCK, Harvey YE, Ray J. MORRIS, and Colin L. WATERS

***Abstract*— The Tasman International Geospace Environment Radar (TIGER) is a SuperDARN HF backscatter radar located on Bruny Island, Tasmania (147.2°E, 43.4°S geographic; –54.6°Λ). HF backscatter radars obtain echoes when the obliquely propagating radio waves achieve normal incidence with magnetic field-aligned irregularities of decametre scale size forming in association with irregularities of scale size 100 m to 1 km. We report the occurrence statistics of nightside auroral and subauroral ionospheric echoes derived from all the normal scan beam 15 soundings made during the one-year interval December 1999 to November, 2000. These sunspot maximum results were sorted into bins of universal time, range, season, and K_p index. The observed variations can be explained by the combined effects of changes in radar operation, changes in the prevailing propagation conditions (including *D*-region absorption and the preferred ranges for backscatter from field-aligned irregularities), and changes in the production and movement of decameter-scale irregularities in the nightside auroral oval controlled by geomagnetic activity and ionospheric conductivity in the radar field-of-view and conjugate ionosphere.**

***Index Terms*—Aurora Australis, ionospheric irregularities, SuperDARN radars**

I. Introduction

THE Tasman International Geospace Environment Radar (TIGER) [1] is a HF backscatter radar located on Bruny Island, Tasmania (147.2°E, 43.4°S geographic; –54.6°Λ geomagnetic). TIGER is a component of the Super Dual Auroral Radar Network (SuperDARN) used to study high-latitude convection [2]. The statistics of echoes detected by other radars in the network have been investigated (e.g., [3], [4]). However, TIGER is the most equatorward of the SuperDARN radars, both geographically and geomagnetically, extending the coverage of the network to include the nightside auroral and subauroral ionosphere for moderate levels of geomagnetic activity. Hence we expect the TIGER statistics to differ from those obtained with the other radars.

Fig. 1 shows the field of view (FOV) of the radar mapped in geographic (blue) and geomagnetic (red) coordinates. TIGER performs one sequential 16-beam scan from east (beam 15) (black) to west (beam 0) in the fast (normal) routine modes of operation, integrating for 3 s (7 s) on each beam. Hence a full scan takes 48 s (112 s), with successive scans synchronised to the start of 1-min (2-min) boundaries.

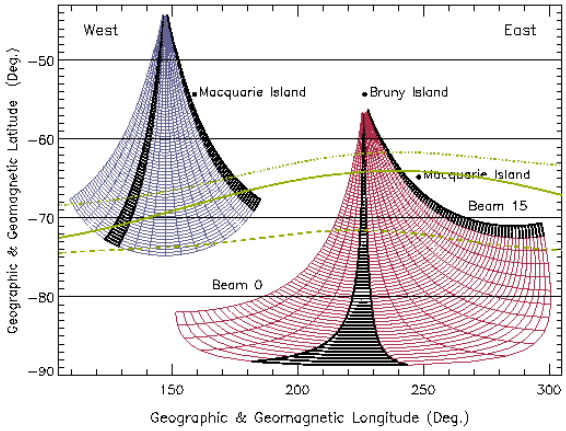

Fig. 1. The field of view (FOV) of the TIGER radar mapped to geographic (blue) and geomagnetic coordinates (red), both drawn on the same grid to emphasise differences. Model auroral oval boundaries (green) [5] for *AL* = –141 nT ($K_p \approx 3–$) [6], and with the radar located at magnetic midnight, are superimposed in magnetic coordinates: poleward boundary of the discrete aurora (dashed curve), equatorward boundary of the discrete aurora (solid curve), and equatorward boundary of the diffuse aurora (dotted curve) .

Manuscript received November 12, 2001. This work was supported by the Australian Research Council, the Australian Antarctic Science Advisory Council, the UK's Natural Environment Research Council, Australian Antarctic Division, DSTO Salisbury, the Ian Potter Foundation, RLM Systems Pty. Ltd, and the State Government of Tasmania.

M. L. Parkinson and P. L. Dyson are with the Department of Physics, La Trobe University, Victoria, 3086, Australia (telephone: 61-3-94791433, e-mail: m.parkinson@latrobe.edu.au).

J. C. Devlin and H. Ye are with the Department of Electronic Engineering, La Trobe University, Victoria, 3086, Australia.

M. Pinnock is with the British Antarctic Survey, Natural Environment Research Council, Cambridge, CB3 OET, U.K.

R. J. Morris is with Atmospheric and Space Physics, Australian Antarctic Division, Kingston, Tasmania 7050, Australia.

C. J. Waters is with the Department of Physics, University of Newcastle, New South Wales, 2038, Australia.

Individual beams in the scan are separated by 3.24°, and the full scan spans 52°.

Fig. 1 shows the large difference between the geographic and magnetic FOVs—some of the underlying dynamics will be characteristic of a high mid-latitude station (e.g., radio propagation, *D*-region absorption, and insolation), yet others will be characteristic of the subauroral, auroral, and polar cap ionosphere. Model auroral oval boundaries given by the Starkov model [5] have been superimposed. The *AL* index used to drive the model was calculated using the conversion between *AL* and K_p given in [6]. The Starkov model was chosen because it has been validated against measurements, and facilitates the straight-forward calculation of the boundaries using simple formulae. However, other models could have been used and would give similar results.

Diurnal, seasonal, and geomagnetic activity variations in the occurrence of decametre-scale irregularities observed in the subauroral, auroral, and polar cap ionosphere were investigated using echoes recorded on TIGER's magnetic meridian pointing beam 4 (black) [7]. The aim of this paper is to perform a more detailed investigation into the occurrence of subauroral and auroral irregularities using echoes recorded on beam 15 (black). In contrast to beam 4, the range window of beam 15 extends from latitude –57°Λ to –72°Λ, providing the most detailed view of the nightside auroral and subauroral ionosphere hitherto obtained with a SuperDARN radar.

Fig. 1 shows that beam 15 becomes a zonal, eastward-looking beam at furthest ranges, actually reaching a maximum latitude of –71.8°Λ (range cell 68) before folding back toward the equator beyond this range. Thus observations made using beam 15 are also very sensitive to narrow channels of fast zonal drifts known to occur in the auroral and subauroral ionosphere, including "subauroral ion drifts," (SAID) [8]. Beam 15 is also the most useful beam for studying a population of near-range auroral echoes with low spectral widths [9]. Because of the alignment of beam 15 with respect to the convecting irregularities, the associated echo powers, Doppler shifts, and spectral widths are often more interesting than when observed on beam 4.

Lastly, in this study we not only aim to understand the behaviour of high-latitude ionospheric irregularities, but also to help quantify the performance of the radar and understand the different features likely to be observed under a broad range of conditions. This will facilitate the design of future experiments and the subsequent analysis of data recording the behaviour of poorly understood electrodynamic processes in the auroral and subauroral ionosphere.

II. Radio Propagation Effects

Variations in the occurrence rates of HF radar echoes are not entirely due to changes in the geophysical conditions directly affecting the production and dissipation of ionospheric irregularities. For example, diurnal, seasonal, and geomagnetic activity variations in the ionospheric electron density profiles encountered along the ray paths will affect the ranges at which coherent echoes can be obtained from field-aligned irregularities. Focussing and defocusing of radio waves as they are refracted through the ionosphere must also be allowed for. The range dependency is also partly due to ionospheric absorption (mostly nondeviative absorption in the *D*-region), and lastly, free-space losses (the familiar divergence of power with range) are also important.

Because of TIGER's relatively low geographic latitude (43.4°S), yet high magnetic latitude (–54.6°Λ), the behaviour of ionospheric absorption at mid- and high-latitudes are both important considerations. Davies [10] reviewed the well known behaviour of absorption at mid-latitudes. Quiet-time ionospheric absorption is influenced by the solar zenith angle at a station, maximising near to when the solar zenith angle is a minimum. Maximum absorption actually occurs ~20 min past noon at mid-latitudes, and residual absorption persists into the night. Absorption also maximises during summer, decreases towards the equinoxes, but an "anomalous" absorption peak related to stratospheric warming occurs during the winter. The solar zenith angle is still an important factor at high latitudes, but the influence of the winter anomaly diminishes. Absorption maximises during the night at auroral latitudes because of energetic particle precipitation. Lastly, solar X-ray flares can lead to the total loss of echoes recorded by even the most sensitive HF radars.

Ray-tracing techniques can be used to quantify the relative variations of ionospheric absorption and the focussing of radio waves by refraction. For example, a companion paper [11] shows an ~20 dB enhancement in the SNR of sea echoes observed near sunset, spring equinox, and propagated via one hop in the *F2* layer. A similar increase in the SNR of radio waves backscattered from ionospheric irregularities, yet propagated via one-and-a-half hops, should occur at the same time.

Variations in all of the preceding effects are comparable to the ~40 dB dynamic range of backscatter power observed using SuperDARN radars, and work continues on quantifying their relative contributions.

III. Observations and Analysis

In the routine mode of operation, SuperDARN radars calculate autocorrelation functions (ACFs) of echoes digitised at 75 range gates starting at 180 km and separated by 45 km (i.e., 180 to 3555 km). The "FITACF" algorithm [12] processes the ACFs to estimate the echo power in logarithmic units of signal-to-noise ratio (SNR) (i.e., dB), line-of-sight Doppler velocity (m s^{-1}), and the Doppler spectral width (m s^{-1}), for all 75 ranges on every beam. Our version of FITACF rejects echoes with SNR<3 dB.

FITACF also flags echoes as ground scatter if the Dopp-

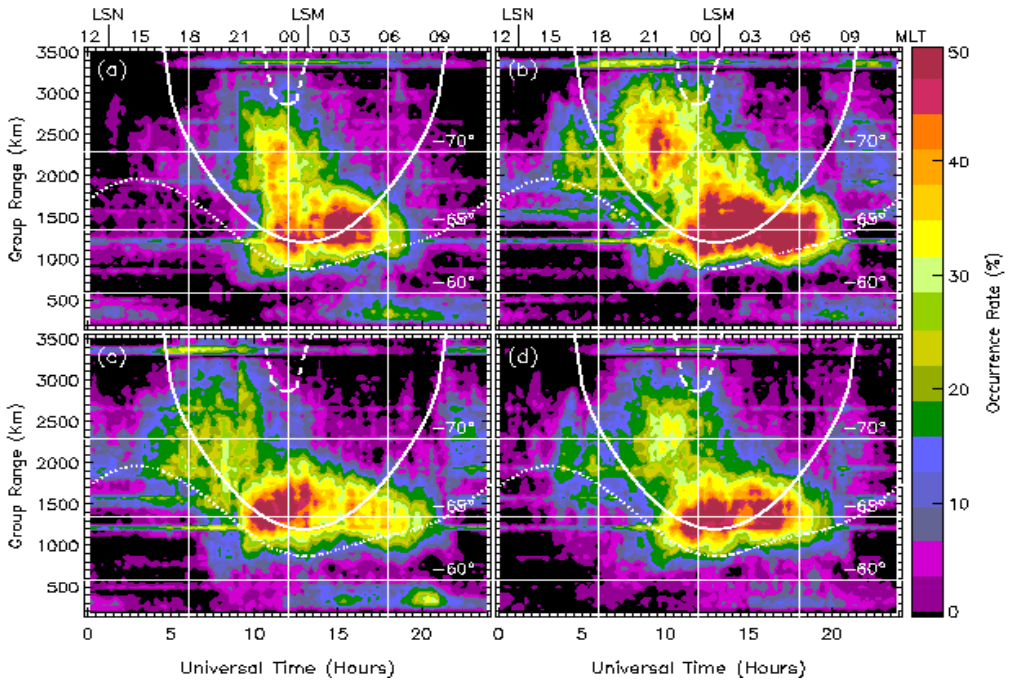

Fig. 2. The occurrence rate of beam 15 ionospheric echoes detected during (a) summer (days 313 to 035), (b) autumn (days 036 to 126), (c) winter (days 127 to 221), and (d) spring (days 222 to 312) for all K_p values. Note there were no 15-min time bins when soundings were not made, so 0% means a zero occurrence rate, not zero observations. As in Fig. 1, auroral oval boundaries for $AL = -141$ nT ($K_p \approx 3-$) have been superimposed. Nominal values of MLT in the ionosphere above Macquarie Island, and local solar noon (LSN) and midnight (LSM) are also shown at the top of the plots.

ler speeds and spectral widths are less than 50 m s^{-1} and 20 m s^{-1}, respectively, and determined with small errors. Of course, by "ground scatter," we usually mean echoes from the Southern Ocean in the case of TIGER. In this study, ionospheric echoes are those defined as such by the FITACF algorithm. This identification is effective in the vast majority of cases, but work continues on quantifying its performance and separating the different kinds of echoes in ambiguous cases.

We compile all the routine mode data (normal_scan_ nodata and normal_scan3) recorded during the first year of radar operation, December 1999 to November, 2000. A total of 1,357,310 ionospheric echoes were identified on 151,310 separate beam 15 soundings, so the major features shown here are statistically significant. The occurrence rates were calculated by counting the total number of echoes during 15-min intervals of universal time (UT) on beam 15 at each of the 75 ranges, then dividing by the total number of soundings actually made. Thus 96 times × 75 ranges = 7200 occurrence rates are calculated for each map showing an average diurnal variation in the following section. The data were further sorted into four different seasons and six categories of the K_p index. For each of these categories the total number of echoes was always divided by the actual number of soundings made. Hence the occurrence rates are "self-normalising" with respect to the chosen category.

Ideally, a SuperDARN radar transmits with 16 transmitters, one for each antenna, but during winter the radar operated with as few as 4 transmitters due to equipment failures. Although many transmitters were quickly repaired, work on all 16 was not completed until well into spring. This meant the radar gain was sometimes lower by ≤12 dB during winter and spring, reducing the dynamic range of echoes from ~40 to ~30 dB. The automatic gain control probably compensated for the loss of SNR to some extent, but a slight reduction in the occurrence rates must have occurred during both seasons.

Results are shown as contour plots versus UT and group range, with values of magnetic latitude superimposed. Nominal values of magnetic local time (MLT) in the ionosphere above Macquarie Island (159.0°E, 54.5°S; –65°Λ), located just to the east of beam 15, are also shown at the top of the plots. Local solar time (LST) is approximately equal to MLT minus 1.3 hours above Macquarie Island.

IV. Results

Fig. 2 shows the occurrence rate of beam 15 ionospheric echoes sorted according to season. Note the seasons were redefined to be roughly centered on the equinoxes and solstices, thereby emphasising the component of variation controlled by solar-zenith angle. As will be shown, the observed variability was only partly related to the solar-zenith angle. Thus we also superimpose a grid of MLT and magnetic latitude, since it is well known that ionospheric convection and irregularity production associated with auroral activity are guided by the Earth's magnetic field, including dipole tilt effects.

To first order, all seasons exhibited similar patterns of echo occurrence, but there were some intriguing differences.

TABLE I
SEASONAL CHANGES IN OCCURRENCE RATES, RANGE >630 KM

	Summer	Autumn	Winter	Spring
Total No. Echoes	287,279	271,211	370,876	333,339
Total No. Beam Soundings	40,231	26,214	44,384	40,481
Average Occur. Rate (%)	10.21	15.32	12.54	11.79
Standard Error (%)	0.15	0.18	0.15	0.15
Peak Occur. Rate (%)	60	66	56	57

TABLE II
SEASONAL CHANGES IN OCCURRENCE RATES, RANGE ≤630 KM

	Summer	Autumn	Winter	Spring
Total No. Echoes	29,444	12,763	32,247	20,146
Total No. Beam Soundings	40,231	26,214	44,384	40,481
Average Occur. Rate (%)	6.14	4.01	6.22	3.97
Standard Error (%)	0.17	0.13	0.17	0.09
Peak Occur. Rate (%)	28	22	34	15

For example, there was a nightside enhancement of echo occurrence confined to ~11 to 17 UT (23 to 05 MLT) and –63°Λ and –67°Λ in summer, but extending from ~11 to 19 UT (22 to 07 MLT) in autumn. There was a lesser, dusk enhancement confined to ~09 to 14 UT (21 to 02 MLT) and –68°Λ to –71°Λ in summer, but extending from ~04 to 15 UT (16 to 03 MLT) in autumn.

Lastly, there was a summer-time enhancement of scatter during 17 to 21 UT (05 to 09 MLT) at approximate ranges ≤630 km (range bin 11) (a). A second enhancement of this near-range scatter occurred during early winter (c). This scatter is generally thought to contain echoes from meteor trails and *E*-region plasma instabilities associated with auroral activity and sporadic *E*. Hence in the following analysis we separate the echoes into two populations, the near-range echoes at ranges ≤630 km (to be discussed), and the far-range echoes at ranges >630 km. The latter are generally thought to correspond to upper *E*- and *F*-region irregularities drifting at the ion convection velocity [13].

Table I shows the total number of far-range (>630 km) echoes observed in each season, the total number of beam 15 soundings in each season, the average occurrence rates, their standard errors, and the peak occurrence rates. Variability in the total number of soundings reflects upon equipment failures (computer crashes, etc.). There are 64 range bins at ranges >630 km. Hence the average occurrence rate (%) is the average of the 96 times × 64 ranges = 6144 occurrence rates calculated for each season. This average does not equal the total number of echoes divided by the total number of beam soundings because there was a different number of soundings in each of the 15-min intervals and 64 ranges. The standard errors (%) were calculated by dividing the standard deviations of the occurrence rates by √6144, and were calculated to reveal the statistical significance of the seasonal changes (the actual spread of occurrence rates in each season was shown in Fig. 2). Lastly, the peak occurrence rate is simply the maximum occurrence rate of the 6144 occurrence rates.

Table I shows the largest number of echoes was recorded during winter (Fig. 2c), then spring (d), summer (a), and least of all during autumn (b). However, due to equipment failures, a different number of beam soundings were made each season. Hence the average occurrence rate was actually largest for autumn, next largest for winter, then spring, and least of all for summer. On the other hand, peak occurrence rates were largest in autumn, then summer, spring, and winter. The seasonal changes are statistically significant, but systematic biases not related to the occurrence of ionospheric irregularities may be present.

Table II compiles the same information as Table I, except it shows the occurrence rates of near-range (≤630 km) echoes. There are 11 range bins at ranges ≤630 km, so an average occurrence rate is the average of 96 times × 11 ranges = 1056 occurrence rates. The occurrence rates were largest (~6.2%) and equal within the error limits during summer and winter, and 2% lower and equal during autumn and spring. The peak occurrence rates showed a similar behaviour, but clearly were a minimum during spring, and a maximum during 20 to 21 UT in winter.

Fig. 3 shows the occurrence rates of ionospheric echoes for all seasons combined, and sorted according to geomagnetic activity, as measured by the K_p index. Peak occurrence rates >50% were usually observed in the nightside ionosphere from ~10 to 19 UT (22 to 07 MLT) and –63°Λ and –67°Λ. For quiet conditions, K_p = 0 to 1 (a), the maximum occurrence was from 09 to 12 UT (21 to 00 MLT) and –69°Λ to –71°Λ, but for K_p >1 to 2 (b), the maximum occurrence shifted equatorward to between –63°Λ and –67°Λ. Thereafter, the band of scatter was "trapped" in this latitude range, except during very disturbed periods (K_p >4) (e), (f) when strong enhancements of near-range scatter began to appear. For the most disturbed periods (K_p >5) (f), there was a lot of near-range *E*-region scatter, and scatter from both near and far ranges became locally intense, but very patchy.

Table III is in the same format as Table I, except it shows the changes in average occurrence rate with the K_p index. The average occurrence rate was smallest during the quietest conditions (Fig. 3a), it grew to a maximum for K_p >4 to 5 (e), and thereafter (f) it fluctuated from interval to interval. Some very large occurrence rates were calculated for K_p >6 (not shown). During the most disturbed intervals (Fig. 3f), the auroral oval began to expand equatorward of

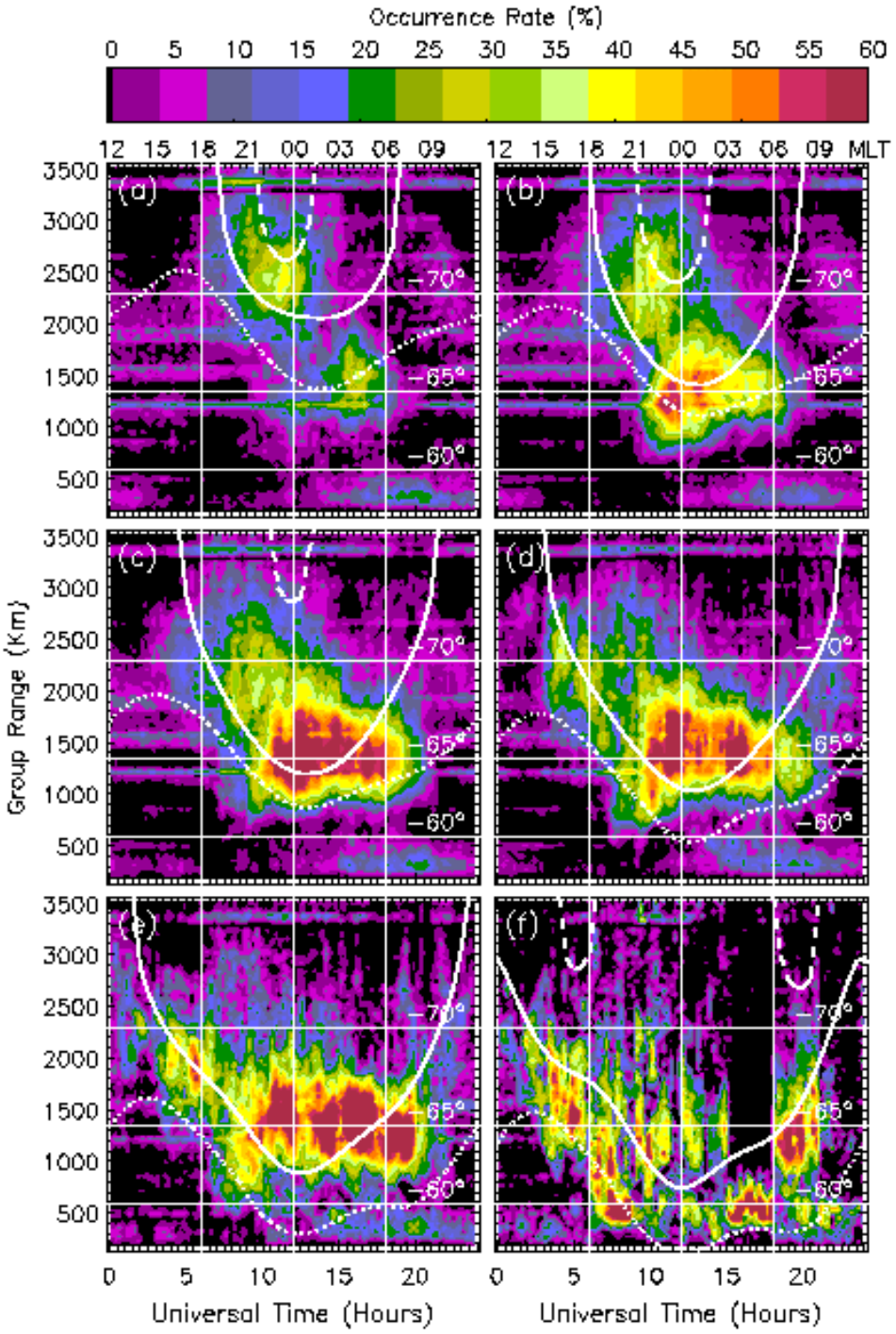

Fig. 3. The occurrence rate of beam 15 ionospheric echoes detected during all seasons, and sorted according to geomagnetic activity. (a) K_p = 0 to 1, (b) K_p >1 to 2, (c) K_p >2 to 3, (d) K_p >3 to 4, (e) K_p >4 to 5, and (f) K_p >5 to 6. Model auroral oval boundaries for AL = −21 nT ($K_p \approx$ 1–) (a), AL = −64 nT ($K_p \approx$ 2–) (b), AL = −141 nT ($K_p \approx$ 3–) (c), AL = −240 nT ($K_p \approx$ 4–) (d), AL = −350 nT ($K_p \approx$ 5–) (e), and AL = −458 nT ($K_p \approx$ 6–) (f) have been superimposed.

the half-hop range window, and near-range auroral *E* echoes may have begun to mask *F*-region scatter at greater ranges.

Table III also shows the peak occurrence rates steadily grew from 43% during the quietest intervals towards 100% during the most disturbed intervals (not shown). This is because the averages were calculated using a smaller and smaller number of intervals encompassing larger and larger geomagnetic storms. Statistics equivalent to those in Table III for near-range (≤600 km) echoes are not shown because there was no significant dependency on geomagnetic activity until K_p >5 when the auroral oval expanded into the near-range bins.

Although the averages for the largest K_p values were only representative of a small number of storms, they clearly showed that localised “hot spots” of echo detection were often observed, even during major storms when intense

TABLE III
GEOMAGNETIC CHANGES IN OCCURRENCE RATES, RANGE >630 KM

K_P	0–1	>1–2	>2–3	>3–4	>4–5	>5–6
Total No. Echoes	190,253	309,490	380,032	219,327	106,575	27,024
Total No. Beam Soundings	31,119	40,257	40,862	22,983	10,224	3,410
Average Occur. Rate (%)	8.07	11.46	13.98	14.17	15.98	10.56
Standard Error (%)	0.10	0.15	0.20	0.19	0.22	0.18
Peak Occur. Rate (%)	43	62	71	75	82	78

precipitation was expected. It seems that absorption due to energetic particle precipitation reduces echo occurrence in transient, spatially localised episodes, but overall the echo occurrence remains high during major storms.

Lastly, the transmitter pulse set was designed to minimise the detrimental effects of range aliasing. However, the narrow, horizontal bands in all panels of Figs. 2 and 3 (including the one centered near range 3375 km) correspond to bad ranges in the ACF analysis.

V. DISCUSSION

From the superimposed auroral oval boundaries [5], we infer that most of the far-range (>630 km) ionospheric echoes observed on beam 15 were associated with decametre-scale irregularity production in the nightside discrete and diffuse auroral ovals. The equatorward boundary of intense irregularity production tended to expand equatorward with increasing levels of geomagnetic activity. The poleward boundary also tended to expand poleward during the most disturbed conditions. However the behaviour of ionospheric echoes detected by TIGER only partly agreed with this behaviour.

Recall that variability in the prevailing propagation conditions including the refraction of the radio waves must influence the observation of ionospheric irregularities. The ionospheric electron density encountered along the ray paths must specify the preferred range windows at which transmitted radio waves achieve normal incidence with magnetically field-aligned irregularities [13]. To produce observable echoes, these preferred range windows must also correspond to ionospheric regions associated with intense irregularity production. The gradient drift instability [14] implies the latter is favoured by large convection velocities parallel to sharp horizontal gradients in *F*-region plasma density.

For the same level of geomagnetic activity, the dusk auroral oval (18 MLT) is found further equatorward than the noon auroral oval (12 MLT), and the midnight auroral oval (00 MLT) is found even further equatorward. Fig. 2 showed two regions of enhanced echo occurrence, one found between –68°Λ and –71°Λ mostly before magnetic midnight, and the other between –63°Λ and –67°Λ persisting beyond magnetic midnight. Comparing Figs. 3 (a) and (e) reveals the range of these two regions differed by nearly a factor of two over the full range of geomagnetic activity. We speculate the two regions of enhanced scatter were observed because the auroral oval expanded through two, partly overlapping range windows favouring the detection of ionospheric irregularities. These range windows correspond to 0.5- and 1.5-hop propagation through disturbed *F*-layers, though some auroral *E* propagation must also have been involved.

However, there is a complementary explanation. Before about 10 UT (22 MLT), only the furthest ranges sampled plasma flows east of the Harang discontinuity, whereas soon afterwards all ranges sampled these flows. The SNR of echoes detected post the Harang discontinuity are often >15 dB stronger [9], implying more intense irregularities circulating within the dawn convection cell. Note that more intense electron precipitation [15] and thermospheric gravity-wave perturbations [16] occur post midnight. Hence the two regions of enhanced echo occurrence are explained by a combination of the prevailing propagation conditions and a dichotomy of irregularity production.

There was an enhancement of high-latitude (–68° to –71°Λ) scatter located near dusk. The subset of this scatter having low spectral widths had characteristics reminiscent of “dusk scatter” associated with the main ionospheric trough [17], but our results also suggest that most of these echoes occur in the auroral oval. Nevertheless, case studies suggest that TIGER often detects bands of true subauroral scatter associated with the main ionospheric trough [8], [9].

Enhanced *D*-region absorption associated with insolation and energetic particle precipitation will also attenuate the propagation of HF radio waves. Part of the lower occurrence rate for the 1.5-hop echoes prior to midnight must also have been due to greater free-space losses and absorption. During all seasons there was a minimum occurrence of echoes in the dayside ionosphere from ~22 to 03 h UT (10 to 15 h MLT), but more dayside echoes were observed during winter, as would be expected if ionospheric absorption were reduced then.

The dayside auroral oval is typically located at ~ –75°Λ, well poleward of the furthest ranges sampled by beam 15.

However, the dayside occurrence rates were also low on beam 4 which almost reaches the corrected geomagnetic pole. Thus greater free-space losses and ionospheric absorption must combine to limit the detection of dayside cusp scatter with the TIGER radar. Signatures of the ionospheric cusp are better observed with SuperDARN radars located further poleward, such as the radar located at Halley Base (333.4°E, 75.5°S; –61.8°Λ), Antarctica.

Scintillation of VHF signals traversing the ionosphere and received with ground-based antennas are caused by ionospheric irregularities of scale size ~250 m to 1 km. Typical power spectra of ionospheric irregularities show a continuum of irregularities from these scale sizes down to the decametre-scale size observed using HF backscatter radar. Hence we expect a correspondence between the occurrence of ionospheric irregularities implied by the two kinds of measurements.

Indeed, the diurnal and seasonal variation of scintillation index observed at Narssarssuaq (+63°Λ) [18], (see Fig. 19 therein) resembles the variation of occurrence rate shown in Fig. 2. Both kinds of data show similar maxima during the night. However, there is a diurnal maximum of scintillations centered pre-midnight (~23 MLT) at Narssarssuaq, whereas the peak occurrence rates are centered post-midnight (~02 MLT) in the TIGER FOV. The Narssarssuaq scintillation index maximises in the months of March and April, and then slowly declines throughout the remainder of the year, reaching a minimum during November and December. A similar but weaker seasonal behaviour was observed using TIGER (Table I), despite the stations residing in different longitude sectors, and opposite hemispheres.

Basu [19] proposed that the changing geometry of the plasma sheet with the dipole tilt angle of the Earth's magnetic field should lead to a weaker seasonal variation observed in the Alaskan longitude sector.

Recall the conductivity of the ionosphere is controlled by the solar zenith angle and energetic particle precipitation at high latitudes. The presence of a conducting *E* region reduces the lifetime of irregularities in the *F* region by allowing the cross-field plasma diffusion to proceed at the faster electron rate, rather than the ion rate [14], [20]. Thus irregularities "dissolve" faster in the presence of a conducting *E* region. Moreover, aurora tend to occur in regions of low ionospheric conductivity [21], and must contribute to the formation of intense irregularities in the auroral oval (as demonstrated by their frequent occurrence therein). Lastly, the conductivity of the conjugate ionosphere must be considered in all of these processes.

Near the winter solstice the nightside ionosphere within the FOV will be in total darkness, whereas the conjugate ionosphere will be strongly illuminated. Near summer solstice the nightside ionosphere within the FOV will be in total darkness for only a short interval, whereas the conjugate ionosphere will be in total darkness. Near the equinoxes the nightside ionosphere within the radar FOV and the conjugate ionosphere will be in total darkness. Hence the ionospheric conductivity at conjugate points will also be low, and auroral activity large. It is also well known that auroral activity maximises near March equinox when the solar declination angle is near zero [22].

The role of ionospheric conductivity in the formation and lifetime of decametre-scale irregularities in the radar FOV needs to be quantified using theoretical models before we make any conclusions. To first order, we might expect the maximum occurrence rates near March equinox, and the minimum occurrence rates during summer. This is similar to the far-range (>630 km) observations. However, the symmetric behaviour of near-range (≤600 km) echoes (Table II), namely nearly equal peak occurrence rates during summer and winter, and nearly equal minimum occurrence rates in autumn and spring, is in closer agreement with the expected effect of conductivity on mid-latitude irregularity occurrence.

The ionospheric echoes observed by SuperDARN radars at far ranges (say, >630 km) are generally thought to originate from upper *E*- and *F*-region irregularities drifting at the ion convection velocity [13]. At present, we do not completely understand variability in the echo occurrence at near ranges (say, ≤630 km), but work continues on separating out the different populations of scientifically useful echoes.

TIGER observations showed the peak occurrence of Leonids meteor during dawn of 18 November, 2001. Most of the meteor echoes, presumably from heights of ~94 km [23], had relatively low Doppler velocities and spectral widths, and so were identified as sea echoes by the current radar analysis program. Indeed, the diurnal variation of near-range "sea echoes" often shows a distribution centered near dawn, as expected for meteors. The near-range ionospheric scatter shown in Fig. 2 also shows enhancements near dawn, as might be expected when large mesospheric winds and turbulent boundary layers disperse the meteor trails.

However, the TIGER elevation angle data suggests that most of the near-range ionospheric scatter originates from the *E* region and bottom-side *F* region where many of the echoes are known to be associated with plasma instabilities [24]. The summer-time morning enhancement of near-range ionospheric scatter (Fig. 2a) might also be associated with the enhancement of sporadic *E*-layer irregularities known to occur at this time [25].

An ionosonde is located at Hobart (close to TIGER), and routinely records the occurrence of sporadic *E*, auroral *E*, and diffuse slant *E*- and *F*-traces. These observations might be compared with TIGER observations of near-range scatter to help separate out the different kinds of echoes, and perhaps even infer an association between meteor ablation and sporadic *E* formation.

In summary, SuperDARN radars can be used to monitor the occurrence of decametre-scale irregularities in the

auroral and subauroral ionosphere, as long as changes in instrumental performance and HF propagation conditions are allowed for. The underlying geophysical processes controlling the formation and lifetime of the irregularities can then be investigated. These processes include the effects of ionospheric convection velocity, horizontal gradients in plasma density due to energetic particle precipitation, and changes in ionospheric conductivity due to insolation and energetic particle precipitation.

From Figs. 2 and 3 we conclude the TIGER radar performs remarkably well during all seasons and under a broad range of geomagnetic activity, as might be expected for a FOV encompassing high geographic mid-latitudes where seasonal variations in solar zenith angle and the effects of energetic particle precipitation are modest relative to those encountered by other radars in the SuperDARN network.

ACKNOWLEDGMENT

We thank the numerous people who contributed to the construction, operation, and maintenance of TIGER. They include Anthony M. Breed, Mark Gentile, Longsong He, Danny Ratcliffe, Paul R. Smith, and Jim Whittington,

REFERENCES

[1] P. L. Dyson and J. C. Devlin, "The Tasman International Geospace Environment Radar," *The Physicist (The Australian Institute of Physics)*, vol. 37, pp. 48-53, March/April, 2000.

[2] R. A. Greenwald, et. al., "DARN/SuperDARN: A global view of the dynamics of high-latitude convection," *Space Sci. Rev.*, vol. 71, pp. 761-796, 1995.

[3] J. M. Ruohoniemi and R. A. Greenwald, "Rates of scattering occurrence in routine HF radar observations during solar cycle maximum," *Radio Sci.*, vol. 32, pp. 1051-1070, 1996.

[4] S. E. Milan, S. E., T. K. Yeoman, M. Lester, E. C. Thomas, and T. B. Jones, "Initial backscatter occurrence statistics from the CUTLASS HF radars," *Ann. Geophysicae*, vol. 15, pp. 703-718, 1997.

[5] G. V. Starkov, "Mathematical model of the auroral boundaries," *Geomag. Aeronomy*, vol. 34, pp. 331-336, 1994

[6] G. V. Starkov, "Statistical dependencies between the magnetic activity indices," *Geomag. Aeronomy*, vol. 34, pp. 101-103, 1994

[7] M. L. Parkinson, J. C. Devlin, M. Pinnock, P. R. Smith, P. L. Dyson, and C. L. Waters, "Rates of occurrence of TIGER HF radar echo parameters sorted according to the K_p index and the interplanetary magnetic field—early results," *Proceedings of the SuperDARN Workshop*, Beechworth, Australia, 22-26 May, 2000.

[8] M. L. Parkinson, M. Pinnock, P. L. Dyson, H. Ye, J. C. Devlin, and M. R. Hairston, "On the lifetime and extent of an auroral westward flow channel observed during a magnetospheric substorm," *Ann. Geophysicae*, submitted for publication.

[9] M. L. Parkinson, P. L. Dyson, M. Pinnock, J. C. Devlin, M. R. Hairston, E. Yizengaw, and P. J. Wilkinson, "Signatures of the midnight open-closed magnetic field-line boundary during balanced dayside and nightside reconnection," *Ann. Geophysicae*, submitted for publication.

[10] K. Davies, *Ionospheric Radio.* IEE Electromagnetic Waves Series 31, London, UK: Peter Peregrinus Ltd., 1990.

[11] P. L. Dyson, R. J. Norman, and M. L. Parkinson, "Ionospheric propagation modes identified using the TIGER HF radar," *Proceedings of the Workshop on the Applications of Radio Science*, Leura, Australia, 20-22 February, 2002 (This issue).

[12] K. B. Baker, et. al., "HF radar signatures of the cusp and low-latitude boundary layer," *J. Geophys. Res.*, vol. 100, pp. 7671-7695, 1995.

[13] J. P. Villain, G. Caudal, and C. Hanuise, "A SAFARI-EISCAT comparison between the velocity of *F* region small-scale irregularities and ion drift," *J. Geophys. Res.,* vol. 90, pp. 8433–8444, 1985.

[14] M. C. Kelley, J. F. Vickrey, C. W. Carlson, and R. Torbert, "On the origin and spatial extent of high-latitude *F* region irregularities," *J. Geophys. Res.*, vol. 87, pp. 4469-4475, 1982.

[15] M. S. Gussenhoven, D. A. Hardy, and N. Heinemann, "Systematics of the equatorward diffuse auroral boundary," *J. Geophys. Res.*, vol. 88, pp. 5692-5708, 1983.

[16] M. Conde, and J. Innis, "Thermospheric vertical wind activity mapped by the Dynamics Explorer-2 satellite," *The Cedar Post*, vol. 43, p. 12, September, 2001.

[17] J. M. Ruohoniemi, J. M., R. A. Greenwald, J-P Villain, K. B. Baker, P. T. Newell, and C.-I. Meng, "Coherent HF radar backscatter from small-scale irregularities in the dusk sector of the subauroral ionosphere," *J. Geophys. Res.*, vol. 93, pp. 12,871-12,882, 1988.

[18] J. Aarons, "Global morphology of ionospheric scintillations," *Proc. IEEE*, vol. 70, pp. 359-378, 1982.

[19] S. Basu, "Universal time seasonal variation of auroral zone magnetic activity and VHF scintillation," *J. Geophys. Res.,* vol. 80, p. 4725, 1975.

[20] J. F. Vickrey and M. C. Kelley, "The effects of a conducting E layer on classical F region cross-field plasma diffusion," *J. Geophys. Res.*, vol. 87, pp. 4461-4468, 1982.

[21] P. T. Newell, R. A. Greenwald, and J. M. Ruohoniemi, "The role of the ionosphere in aurora and space weather," *Rev. Geophys.*, vol. 39, pp. 137-149, 2001.

[22] C. T. Russel, and R. L. McPherron, "Semiannual variation of geomagnetic activity," *J. Geophys. Res.*, vol. 78, pp. 92-108, 1973.

[23] G. E. Hall, J. W. MacDougall, D. R. Moorcroft, J.-P. St.-Maurice, A. H. Manson, and C. E. Meek, "Super Dual Auroral Radar Network observations of meteor echoes," *J. Geophys. Res.*, vol. 102, pp. 14,603-14,614, 1997.

[24] J. P. Villain, R. A. Greenwald, K. B. Baker, and J. M. Ruohoniemi, "HF radar observations of *E* region plasma irregularities produced by oblique electron streaming," *J. Geophys. Res.*, vol. 92, pp. 12,327–12,342, 1987.

[25] J. D. Whitehead, "Recent work on mid-latitude and equatorial sporadic-*E*," *J. Atmos. and Terr. Phys.*, vol. 51, pp. 401-424, 1989.